

Helioseismological constraint on solar axion emission

H. Schlattl and A. Weiss

Max-Planck-Institut für Astrophysik, Karl-Schwarzschild-Str. 1, 85740 Garching, Germany

G. Raffelt

Max-Planck-Institut für Physik (Werner-Heisenberg-Institut), Föhringer Ring 6, 80805 München, Germany
(April 2, 2022)

Helioseismological sound-speed profiles severely constrain possible deviations from standard solar models, allowing us to derive new limits on anomalous solar energy losses by the Primakoff emission of axions. For an axion-photon coupling $g_{a\gamma} \lesssim 5 \times 10^{-10} \text{ GeV}^{-1}$ the solar model is almost indistinguishable from the standard case, while $g_{a\gamma} \gtrsim 10 \times 10^{-10} \text{ GeV}^{-1}$ is probably excluded, corresponding to an axion luminosity of about $0.20 L_\odot$. This constraint on $g_{a\gamma}$ is much weaker than the well-known globular-cluster limit, but about a factor of 3 more restrictive than previous solar limits. Our result is primarily of interest to the large number of current or proposed search experiments for solar axions because our limit defines the maximum $g_{a\gamma}$ for which it is self-consistent to use a standard solar model to calculate the axion luminosity.

PACS numbers: 14.80.Mz, 96.60.Ly

I. INTRODUCTION

Stars are powerful sources for low-mass weakly interacting particles. The backreaction of this energy-loss channel on the properties and evolution of stars has been extensively used to constrain nonstandard neutrino couplings and the properties of axions and other hypothetical particles [1]. While the Sun no doubt is the star best known to us, it does not provide the most restrictive limits on new particle properties. Still, it remains of interest what the Sun can tell us about nonstandard particle-physics assumptions.

Much has improved in our knowledge of the Sun over the past decade because its interior properties have become accessible by helioseismological methods and by a host of solar neutrino experiments. It used to be that a solar model was fixed by adjusting its presolar helium abundance and the mixing-length parameter such as to reproduce the observed luminosity and radius at an age of about 4.6×10^9 years. In this way even rather dramatic modifications could be accommodated. For example, a nonstandard energy-loss channel in the form of axion emission could have been essentially as large as the solar photon luminosity so that the present-day Sun could have been close to its main-sequence turn-off [2]. Naturally, one expects that the precise helioseismological sound-speed profiles which have become available over the past few years will provide far more severe restrictions on possible present-day solar models.

As a specific example for a nonstandard energy-loss channel we consider the Primakoff conversion of axions in the Coulomb fields of charged particles, $\gamma + Ze \rightarrow Ze + a$ (Fig. 1). This case is of particular interest because one can search for the solar axion flux by the reverse process where an axion oscillates into an X-ray in a long dipole magnet which has been oriented toward the Sun,

the so-called “helioscope” method [3,4]. An alternative approach uses the Primakoff backconversion in a germanium crystal where one can achieve a large enhancement in some directions in analogy to Bragg diffraction [5]. In either case it is of interest to know the maximum axion-photon coupling strength which is compatible with well-established solar properties. For example, an early experimental search for solar axions [6] was not sensitive enough to detect these particles even if the coupling strength had been so large as to push the present-day Sun close to its main-sequence turn-off. Put another way, the limit found in this early experiment was not self-consistent in that it required a larger axion emission from the Sun than is compatible with its age. A surprisingly large number of current [7,8] and proposed [9,10] solar axion search experiments has recently emerged. This experimental activity motivates us to examine solar axion limits in the light of helioseismological information.

In Sec. II we describe our standard solar model and compare it with recent helioseismological data. In Sec. III we construct models of the present-day Sun including axionic energy losses and derive a new solar limit on the axion-photon coupling constant. In Sec. IV we discuss our results in the light of other astrophysical limits and in the context of solar axion search experiments.

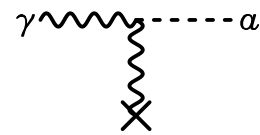


FIG. 1. Primakoff production of axions in the Sun.

II. SOLAR AND SEISMIC MODEL

The solar model used in this paper was computed with the GArching SOlar Model (GARSOM) code, which has been described in its numerical and basic physical details elsewhere [11]. It was shown [12] that it agrees in its gross features with other contemporary up-to-date standard solar models. In particular, it uses the latest OPAL opacities and equation of state [13,14] and takes into account particle diffusion of hydrogen, helium and a number of heavier elements (e.g. C, N, O). We usually follow the evolution beginning from the pre-main sequence to an age of 4.57Gyr (“best model”). To derive the differential effect of axion emission on solar models it is, however, sufficient to calculate models including only H/He-diffusion starting from the zero-age main sequence (ZAMS).

The main difference to other comparable solar models is our treatment of the atmosphere and the outermost superadiabatic convective layers down to an optical depth of 1000, where the stratification of a two-dimensional hydrodynamical simulation [15] is used. In the deeper layers convection is treated according to Ref. [16] even though the temperature gradients are almost perfectly adiabatic and thus independent of the convection theory.

Since the first publication of our solar model [11] the code has been revised. Apart from some minor details the following numerical treatments have been changed: particle diffusion and the nuclear network are now solved simultaneously in the same system of equations instead of following a sequence of burning-mixing-burning between two models of successive age. The opacity interpolation (a two-dimensional bi-rational spline with one free parameter) now resembles closely a standard cubic-spline interpolation, because we found that the strong spline damping we previously used to prevent unphysical oscillations of the interpolation function degraded the agreement of our models with seismic ones [17]. Furthermore, the reaction rate for ${}^3\text{He}({}^3\text{He}, 2p){}^4\text{He}$ [18] and the solar radius ($R_\odot = 6.95508 \times 10^{10} \text{ cm}$ [19]) were updated.

Theoretical solar models are compared with seismic ones which are constructed by the so-called inversion method from measured p-mode frequencies. In Fig. 2 we show the difference in sound speed of our best solar model (solid line) compared to the seismic model from [20]. The dashed line shows a solar model which was calculated from the ZAMS including only H/He-diffusion ($g_{10} = 0$). The latter is used in the following as reference model to illustrate the effect of axion emission. The shaded area shows the uncertainty of the derived profile of the sound speed (c_s) according to Ref. [21]. They were quoting the errors in the quadratic isothermal sound speed. To get the respective errors in c_s we neglect the uncertainties from the adiabatic index Γ_1 , as these contribute barely to the total error [22]. There are three sources for the total uncertainty: (i) the errors of the measured frequencies; (ii) the dependence of the final seismic model on the starting model; and finally, (iii) the uncertainties

in the regularization procedure of the inversion method. The three uncertainties were determined in a conservative way: each error interval was doubled and then their absolute values were added [21]. This was done because the parameter study may not have been exhaustive. The measured frequencies being very precise, the main uncertainties arise from the inversion method itself. Previous studies by [22] found an uncertainty of approximately 5×10^{-4} for $0.2 < r/R_\odot < 0.8$ for each of the three error sources quoted above. Applying the same procedure for determining the conservative errors gives a value of 3×10^{-3} slightly bigger than the uncertainties found by [21]. [23] remark that seismic models do not really constrain solar model for $r/R_\odot < 0.05$.

The deviation of our standard solar model from the seismic model by [20] (solid line in Fig. 2) remains almost everywhere within the error range. The deviation is very similar to that of other comparable solar models in the literature. In particular, we also find a large deviation immediately below the convective zone which might be indicative for either a slight error in the opacities or for overly effective helium diffusion out of the convective envelope [24].

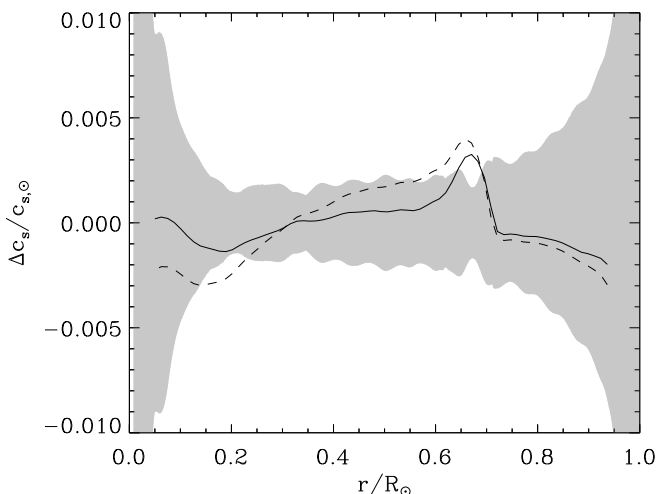


FIG. 2. Difference in sound-speed profiles of present-day solar models compared to the seismic model. The shaded area reflects the uncertainty in the inferred sound speed of the seismic model. The solid line shows our best solar model, the dashed line the reference model ($g_{10} = 0$) used for our analysis.

In the first row of Table II we list the expected counting rates for the gallium and chlorine experiments as well as the flux of ${}^8\text{B}$ neutrinos at the (Super)Kamiokande detector. Assuming flavor conversion of two neutrino types as the solution of the solar neutrino puzzle we show the parameter space in Fig. 5 for which the measured neutrino fluxes of all experiments are reproduced. The upper panel shows the MSW-solutions [25], the lower one the solution for vacuum oscillations (shaded areas). In

the calculation of the MSW-solutions we include the average earth-regeneration effect [26], and for the vacuum-oscillations the annual Sun-Earth distance variation. Our 95% confidence level regions agree with those in the literature.

We have verified by test calculations that including metal diffusion and the new value for $S_{17}(0)$ of the ${}^7\text{Be}(p, \gamma){}^8\text{B}$ reaction of 0.019 keV barn [27] instead of 0.0224 keV barn [28] leads to almost the same parameter regions in the Δm^2 - $\sin^2 2\theta$ -plane as for the reference solar model.

III. SOLAR MODELS WITH AXION LOSSES

We now calculate self-consistent solar models where we include energy losses by axion emission from zero age to the present-day Sun including only H/He-diffusion. Axions [29] generically have a two-photon coupling vertex in full analogy to neutral pions. The interaction Lagrangian can be written in the form

$$\mathcal{L}_{a\gamma} = g_{a\gamma} \mathbf{B} \cdot \mathbf{E} a, \quad (1)$$

where $g_{a\gamma}$ is a constant with the dimension (energy) $^{-1}$, \mathbf{E} and \mathbf{B} are the electric and magnetic fields, and a is the axion field. In keeping with previous works we will always use the dimensionless parameter

$$g_{10} \equiv g_{a\gamma}/10^{-10} \text{ GeV}^{-1} \quad (2)$$

to characterize the coupling strength. The energy-loss rate as a function of g_{10} is discussed in Appendix A.

In Table I we summarize the characteristics of the solar models which include axion losses for several values of g_{10} . We show the present-day axion luminosity L_a ,

TABLE I. Solar models with axion losses.

g_{10}	L_a/L_\odot	Y	Y_c	ρ_c [g/cm 3]	T_c [10 7 K]	$ \Delta c_s/c_{s,0} _{\max}$
0	0	0.266	0.633	153.8	1.563	0.00%
4.5	0.04	0.265	0.641	158.0	1.575	0.16%
10	0.20	0.257	0.679	177.5	1.626	0.81%
15	0.53	0.245	0.751	218.3	1.722	1.82%
20	1.21	0.228	0.914	324.2	1.931	3.12%

TABLE II. Neutrino detection rates.

g_{10}	Ga [SNU]	Cl [SNU]	${}^8\text{B}$ [10 6 s $^{-1}$ cm $^{-2}$]
0	127	8.0	5.5
4.5	136	9.3	6.6
10	184	17.6	13.0
15	323	48	37
20	806	161	127

the presolar helium abundance Y , and the helium abundance, density, and temperature at the solar center. In Fig. 3 we show the deviation of the sound speed profiles of the axionic solar models from a model without axion loss ($g_{10} = 0$). This deviation shows a local maximum at around $r \approx 0.1 R_\odot$, a region where both the models are most sensitive to axion emission and the seismic models are well-constrained. The fractional deviation $|\Delta c_s/c_{s,0}|_{\max}$ at this local maximum is listed in Table I.

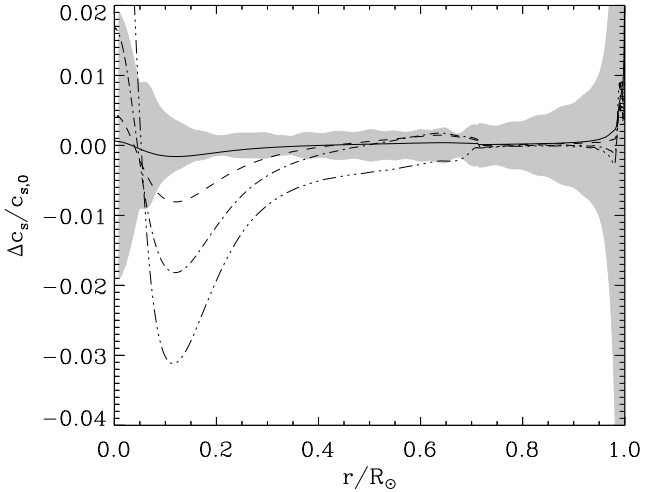


FIG. 3. Difference in sound-speed profiles of present-day solar models with axion losses compared to the reference model in the sense (Reference–Model)/Reference. Different line types correspond to different values of the axion-photon coupling constant: $g_{10}=4.5$ (solid line), 10 (short-dashed), 15 (dash-dotted), 20 (dash-dot-dot-dotted). The shaded area is the same as in Fig. 2.

In Fig. 4 we show the helium profiles of our axionic solar models. The depth of the convective envelope is affected very little by the axion loss—all models are within the value predicted from helioseismology of 0.710–0.716 R_\odot [30]. On the other hand, the present surface helium content depends on the initial one, reduced by diffusion in the course of the evolution by about 0.03. Axionic models with $g_{10} \geq 10$ have a surface helium abundance significantly lower than 0.238, the smallest value allowed from helioseismology [21].

The additional energy sink also affects the present-day core structure (Table I) and thus the solar neutrino flux. The expected neutrino rates are given in Table II for all current experiments. Consequently, the neutrino-oscillation parameters Δm^2 and $\sin^2 2\theta$, for which the measurements are reproduced, depend on g_{10} . For several values of g_{10} we show in Fig. 5 the 95% confidence regions for the MSW and vacuum solutions of the solar neutrino problem. The two MSW-solutions (usually called small and large mixing angle solutions) move toward each other with increasing axion loss. In the case of $g_{10}=15$ there remains only one solution.

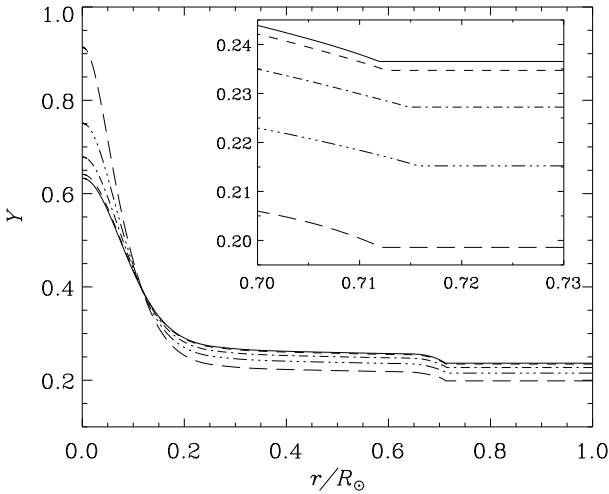


FIG. 4. Helium profiles of present-day solar models with different axion losses. The insert shows a magnification of the region around the bottom of the convective envelope. The line styles correspond to those of Fig. 2.

To illustrate that for $g_{10} \geq 15$ the allowed neutrino parameters fit only very poorly the experimental values we show in Fig. 6 the predicted event rates or neutrino fluxes for GALLEX/SAGE, Homestake and (Super)Kamiokande. For each value of g_{10} the expected rates for the best-fit small-mixing-angle (SMA), large-mixing-angle (LMA) and vacuum (VAC) solution are shown. The error bars reflect the theoretical uncertainties in the predicted rates, the shaded band the measurement errors [31]. In particular, the result from (Super)Kamiokande disfavours any neutrino oscillation solution for $g_{10} \geq 15$. Additionally, the absence of an observed day-night effect in Super-Kamiokande excludes the region between the SMA and LMA solution of a standard solar model ($g_{10}=0$). Including this result would lead to SMA and LMA solutions for $g_{10} \geq 10$ which reproduce the measured rates even worse.

IV. DISCUSSION AND SUMMARY

We have calculated a series of self-consistent solar models with varying amounts of axionic energy losses. For an axion-photon coupling $g_{10} \leq 4.5$, corresponding to an axion luminosity $L_a \leq 0.04 L_\odot$, the small modification of the solar model is well within the uncertainties of all current solar observables. On the other hand, for $g_{10} \geq 10$, corresponding to $L_a \geq 0.20 L_\odot$, the modifications are so significant that it is unlikely that they can be compensated by uncertainties of standard-model input parameters such as the opacities, nuclear fusion rates, age or metal abundance.

Our best solar model deviates from the seismic model at most by $\approx 0.15\%$, just within the generous uncertain-

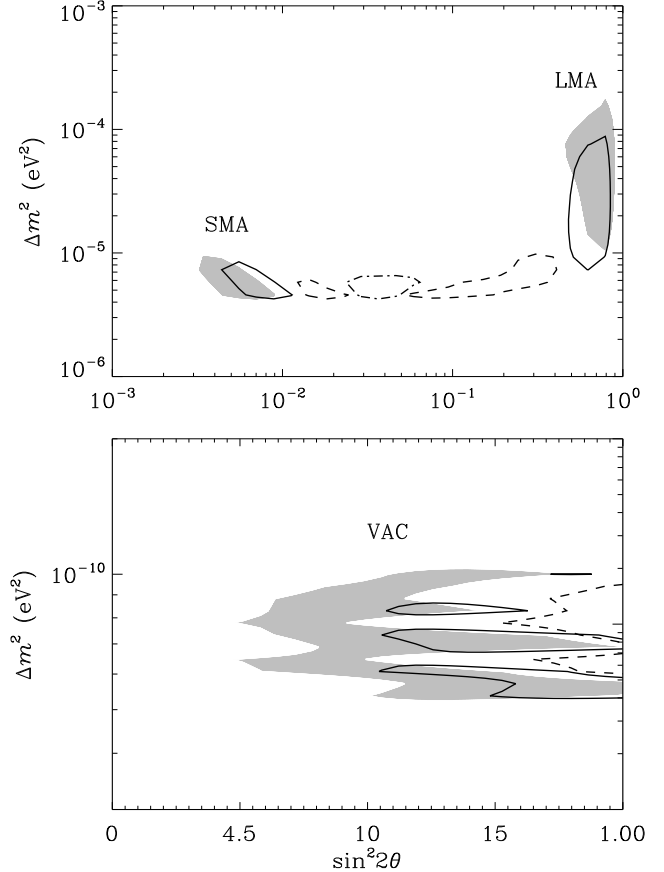


FIG. 5. Neutrino mixing parameters in a two-flavor oscillation scheme where the predicted fluxes agree with the measurements in the GALLEX/SAGE, Homestake and (Super)Kamiokande experiments. The shaded regions and contours are the allowed regions at 95% C.L. for different axion losses ($g_{10} = 0$ shaded, 4.5 solid, 10 dashed and 15 dash-dotted line). For the sake of clarity we omit the vacuum solution for $g_{10}=15$.

ties of the seismic model. To constrain the axion-photon coupling through helioseismology we thus only take into account the differential effect of axion emission on solar models (Fig. 3). For $g_{10} = 10$, the sound speed deviates from the reference model by 0.8% at the local maximum of the deviation at $r \approx 0.1 R_\odot$. This is probably too much to be absorbed by uncertainties in the input physics of the standard solar model.

New measurements from MDI/SOHO providing more accurate low-l frequencies should enable us to get a more precise determination of the sound speed in the central parts. But as the difference of the model with $g_{10} = 4.5$ to the reference model ($g_{10} = 0$) is very small everywhere in the interior, these new frequencies should have almost no influence on our limits.

Further, the $g_{10} \geq 10$ models produce less than 0.227 for the surface helium abundance, while the smallest value allowed by helioseismology is 0.238. Put another way, we may no longer adjust the presolar helium abun-

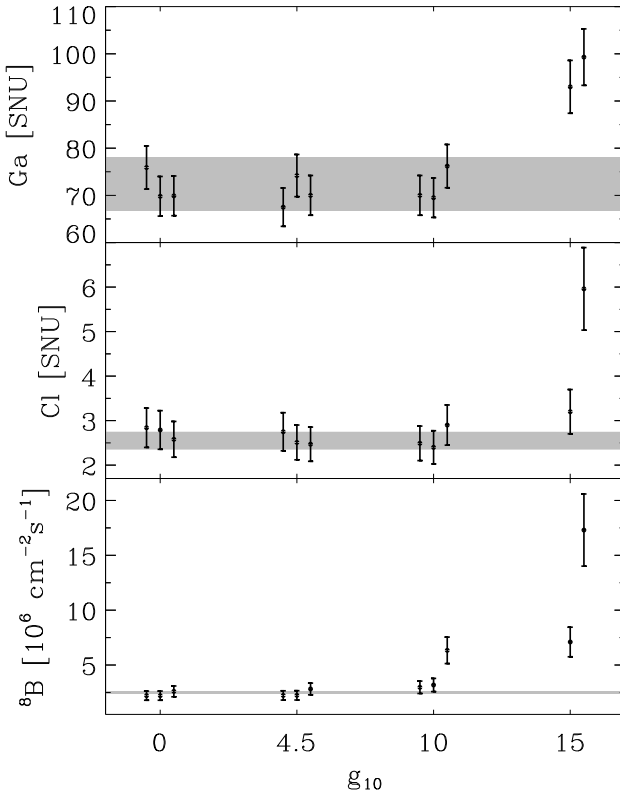


FIG. 6. Expected rates for GALLEX/SAGE, Homestake and (Super)Kamiokande for different solutions and axion losses. Theoretical uncertainties are shown by 1σ -error bars. For each $g_{10} \leq 10$ we plot the SMA, LMA and VAC solutions from left to right; for $g_{10} = 15$ the SMA and LMA cases have merged. The shaded bands represent the 1σ -range of the measured rates.

dance to any desired value to absorb the effect of axion losses on the solar model because the modified helium abundance is not compatible with seismological properties of the convection layers.

Finally, solar models with $g_{10} \geq 10$ produce such large neutrino fluxes that the measured values cannot plausibly be explained by neutrino oscillations. While oscillations are not yet fully established as the undisputed explanation of the measured solar neutrino flux deficits, it is certainly not true that any neutrino flux can be absorbed by suitably adjusted mixing parameters.

In summary, we believe that our present knowledge of the Sun excludes an axion-photon coupling in excess of $g_{10} = 10$, corresponding to $L_a = 0.20 L_\odot$, even if we cannot assign a statistically meaningful confidence level to this bound. This improves the previous solar limit [2] of $g_{10} \lesssim 25$ by about a factor of 3. While other exotic energy-loss channels would have a different energy and temperature dependence, it is probably generic that helioseismology excludes any such channel much in excess of the $0.2 L_\odot$ level.

A recent helioscope experiment to search for solar ax-

ions has reported a limit of $g_{10} < 6$, valid for $m_a \lesssim 0.03$ eV [7]. Therefore, in this mass range the helioscope limit improves our bound and thus is self-consistent, i.e. its validity does not depend on an axion luminosity in excess of what is allowed by the properties of the Sun.

Our new helioseismological bound is much weaker than the well-known limit $g_{10} \lesssim 0.6$ which has been derived from globular-cluster stars [1,2]. We still think it is useful to have independent information from the Sun, especially as the experimental accuracy of solar observations is orders of magnitude better than for every other star. Most importantly, the Sun serves as a source for experimental axion searches. Note that a proposed helioscope experiment using a decommissioned LHC test magnet could conceivably reach the globular-cluster limit [10].

ACKNOWLEDGMENTS

This work is based on a chapter of a thesis to be submitted by H.S. to the Technische Universität München in partial fulfillment of the requirements for a doctoral degree. Partial support by the Deutsche Forschungsgemeinschaft under grant No. SFB 375 is acknowledged. We are grateful to S. Degl'Innocenti for providing us the uncertainties in the radial sound speed profile. Further we would like to thank Dr. J.N. Bahcall for instructive comments.

APPENDIX A: ENERGY-LOSS RATE

The axionic energy-loss rate of a nondegenerate plasma by the Primakoff effect was calculated in Ref. [32]. We follow the representation given in Ref. [1],

$$\epsilon = \frac{g_{a\gamma}^2}{4\pi} \frac{T^7}{\rho} F(\kappa^2) = 0.892 \times 10^{-3} \text{ erg g}^{-1} \text{ s}^{-1} g_{10}^2 T_7^7 \rho_2^{-1} F(\kappa^2), \quad (\text{A1})$$

where $T_7 \equiv T/10^7$ K and $\rho_2 \equiv \rho/10^2$ g cm $^{-3}$. Screening effects are described by the dimensionless function

$$F(\kappa^2) = \frac{\kappa^2}{2\pi^2} \int_0^\infty dx \frac{x}{e^x - 1} \times \left[(x^2 + \kappa^2) \ln \left(1 + \frac{x^2}{\kappa^2} \right) - x^2 \right], \quad (\text{A2})$$

which is shown in Fig. 7. Here,

$$\kappa^2 = \pi\alpha \frac{n_B}{T^3} \left(Y_e + \sum_j Z_j^2 Y_j \right) = 16.56 \rho_2 T_7^{-3} \left(Y_e + \sum_j Z_j^2 Y_j \right), \quad (\text{A3})$$

where $\alpha = 1/137$ is the fine-structure constant, n_B the baryon density, Y_e the number of electrons per baryon,

Y_j the number of nuclear species j per baryon and Z_j its charge number. In a standard solar model $\kappa^2 = 12$ throughout the Sun with a variation of less than 15%, corresponding to $F(12) = 1.842$. A good fit in this region is given by

$$F(\kappa^2) = 1.842 (\kappa^2/12)^{0.31}, \quad (\text{A4})$$

which is shown as a dotted line in Fig. 7.

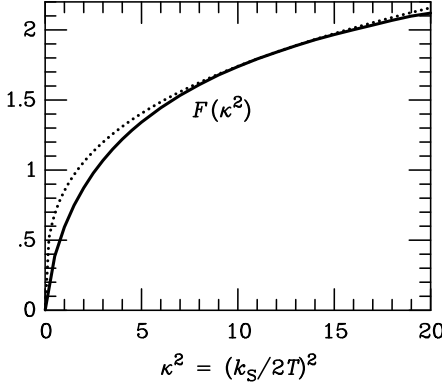


FIG. 7. Function $F(\kappa^2)$, solid line exact result according to Eq. (A2), dotted line our approximation of Eq. (A4).

- [1] G. Raffelt, *Stars as Laboratories for Fundamental Physics*, (Chicago University Press, Chicago, 1996).
- [2] G.G. Raffelt and D.S.P. Dearborn, Phys. Rev. D **36**, 2211 (1987).
- [3] P. Sikivie, Phys. Rev. Lett. **51**, 1415 (1983); (E) ibid. **52**, 695 (1984).
- [4] K. van Bibber, P.M. McIntyre, D.E. Morris and G.G. Raffelt, Phys. Rev. D **39**, 2089 (1989).
- [5] W. Buchmüller and F. Hoogeveen, Phys. Lett. B **237**, 278 (1990). E.A. Paschos and K. Zioutas, Phys. Lett. B **323**, 367 (1994). R.J. Creswick et al., Phys. Lett. B **427**, 235 (1998).
- [6] D.M. Lazarus et al., Phys. Rev. Lett. **69**, 2333 (1992).
- [7] S. Moriyama et al., Phys. Lett. B. **434**, 147 (1998). S. Moriyama, Ph.D. Thesis (in English), University of Tokyo, 1998.
- [8] F.T. Avignone III et al. (SOLAX Collaboration), astro-ph/9708008, submitted to Phys. Lett. B. A.O. Gattone et al. (SOLAX Collaboration), Nucl. Phys. Proc. Suppl. **70**, 59 (1999).
- [9] P.V. Vorobev and I.V. Kolokolov, astro-ph/9501042, unpublished.
- [10] K. Zioutas et al., astro-ph/9801176, submitted to Nucl. Instrum. Meth. A.
- [11] H. Schlattl, A. Weiss, H.-G. Ludwig, Astron. Astrophys. **322**, 646 (1997).
- [12] S. Turck-Chièze et al., to appear in *Structure and Dynamics for the Sun and Sun-like Stars*, 1998, edited by

- S.G. Korzennik and A. Wilson, ESA SP-418 (ESA Publications Division, Noordwijk, Netherlands).
- [13] F.J. Rogers, F.J. Swenson and C.A. Iglesias, Ap. J. **456**, 902 (1996).
- [14] C.A. Iglesias and F.J. Rogers, Ap. J. **464**, 943 (1996).
- [15] B. Freytag, H.-G. Ludwig and M. Steffen, Astron. Astrophys. **313**, 497 (1996).
- [16] V. Canuto and I. Mazzitelli, Ap. J. **370**, 295 (1991); ibid. **389**, 724 (1992).
- [17] H. Schlattl and A. Weiss, in *Neutrino Astrophysics*, Proc. 4th SFB-375 Ringberg Workshop, 1997, edited by M. Altmann, W. Hillebrandt, H.-Th. Janka and G.G. Raffelt (1998), TU München, p. 19.
- [18] M. Junker et al. (LUNA-Collaboration), Phys. Rev. C **57**, 2700 (1998).
- [19] T.M. Brown and J. Christensen-Dalsgaard, Ap. J. **500**, L195 (1998).
- [20] S. Basu et al., MNRAS **292**, 243, (1997).
- [21] S. Degl'Innocenti, W.A. Dziembowski, G. Fiorentini and B. Ricci, Astrop. Phys. **7**, 77 (1997).
- [22] H.M. Antia, Astron. Astrophys. **307**, 609 (1996).
- [23] H.M. Antia and S.M. Chitre, Astron. Astrophys. **339**, 239 (1998).
- [24] O. Richard, S. Vauclair, C. Charbonnel and W.A. Dziembowski, Astron. Astrophys. **312**, 1000 (1996).
- [25] S.P. Mikheyev and A.Yu. Smirnov, Sov. Jour. Nucl. Phys. **42**, 913 (1985). L. Wolfenstein, Phys. Rev. D **17**, 2369 (1978).
- [26] J. Bouchez et al., Z. Phys. C **32**, 499 (1986). M. Cribier, W. Hampel, J. Rich and D. Vignaud, Phys. Lett. B **182**, 89 (1986). A.J. Baltz and J. Wesener, Phys. Rev. D **35**, 528 (1987); ibid. **37**, 3364 (1988). A. Dar, A. Mann, Y. Melina and D. Zajfman, Phys. Rev. D **35**, 3607 (1987). A. Dar and A. Mann, Nature (London) **325**, 790 (1987). S.P. Mikheyev and A.Yu. Smirnov, in *Moriond '87*, Proceedings of the 7th Moriond Workshop on New and Exotic Phenomena, Les Arcs, 1987, edited by O. Fackler and J. Trần Thanh Vân (Frontières, Paris, 1987), p. 405. M.L. Cherry and K. Lande, Phys. Rev. D **36**, 3571 (1987). S. Hiroi, H. Sakuma, T. Yanagida and M. Yoshimura, Phys. Lett. B **198**, 403 (1987); Prog. Theor. Phys. **78**, 1428 (1987). M. Spiro and D. Vignaud, Phys. Lett. B **242**, 279 (1990).
- [27] E.G. Adelberger et al., Rev. Mod. Phys. **70**, 1265 (1998).
- [28] V. Castellani et al., Phys. Rev. D **50**, 4749 (1994).
- [29] J.E. Kim, Phys. Rept. **150**, 1 (1987). H.-Y. Cheng, Phys. Rept. **158**, 1 (1988). M.S. Turner, Phys. Rept. **197**, 67 (1990). G.G. Raffelt, Phys. Rept. **198**, 1 (1990).
- [30] J. Christensen-Dalsgaard, D.O. Thompson and D.O. Gough, Ap. J. **378**, 413 (1991).
- [31] J.N. Bahcall, P.I. Krastev, and A.Yu. Smirnov, Phys. Rev. D **58** 096016 (1998).
- [32] G.G. Raffelt, Phys. Rev. D **33**, 897 (1986).